I&EC research
Industrial & Engineering Chemistry Research

Article

pubs.acs.org/IECR

Complete Equation-Oriented Approach for Process Analysis and Optimization of a Cryogenic Air Separation Unit

Qiwen Fu,[†] Lingyu Zhu,[*,‡] and Xi Chen[*,†]

[†]State Key Lab of Industrial Control Technology, College of Control Science and Engineering, Zhejiang University, 38 Zheda Road, Hangzhou 310027, China

[‡]College of Chemical Engineering, Zhejiang University of Technology, Hangzhou 310014, China

ABSTRACT: A cryogenic air separation unit produces large volumes of high-purity oxygen, nitrogen, and argon through distillation. Such a complex process with a heat-coupling design, a high purity requirement, and a large-scale feature is difficult to analyze and optimize. In this study, a complete equation-oriented (EO) model, which includes a unit model and a thermodynamic model, is developed for cryogenic air separation involving a low-pressure column, a high-pressure column, and an argon side arm column. The EO approach is then applied to deal with the following three issues in air separation: thermodynamic parameter estimation, process analysis with heat-coupling design, and process optimization with varying load demands. The proposed EO method is superior to traditional sequential modular based commercial software in terms of convergence performance.

1. INTRODUCTION

A cryogenic air separation unit (ASU) is an important industrial process that generates high-purity gaseous and liquid products.[1,2] It provides an efficient and cost-effective method of supplying a large amount of gases to processes in metallurgy, chemical and petrochemical industries, and power engineering. When equipping an ASU to iron and steel plants, the load must be frequently changed because of the batch operating feature of such plants. Process analysis and optimization are thus important for operating an ASU; but it is also challenging for such a complex process with a heat-coupling design, a high purity requirement, and a large-scale feature.

A thermo-coupling design is a key feature of cryogenic air separation. Numerous studies have focused on the synthesis of thermo-coupling flowsheets and structures to save energy and improve economic performance. Kansha et al.[3] proposed a novel cryogenic air separation technique based on self-heat recuperation to reduce energy consumption. Fu et al.[4] extended the self-heat recuperation technology to an integrated gasification combined cycle system. Rong et al.[5,6] proposed several specific thermally coupled configurations of multiple component mixtures. Huang et al.[7,8] considered internal heat integration in the design of reactive distillation columns. Incremental coupled heat and material streams complicate optimization because of their narrowed feasible region and strict specifications. Search methods based on rigorous models were also investigated. Zhu et al.[9] applied a homotopy-based backtracking method for simulating and optimizing ASUs to ensure convergence. Time consumption is not a significant issue in process design or synthesis; however, calculation time is always considered for real-time optimization in operations, such as during a rapid and effective search for a new operation point generated by a frequent fluctuation in product demand. Other researchers proposed various methods to simplify the rigorous model for computation. Sirdeshpande et al.[10] represented the mass and energy balances for air separation by using a simplified algebraic model. Bian et al.[11] developed a reduced-order dynamic models for the upper column of an air separation plant. Kamath et al.[12] proposed a group method for complex distillation systems in large-scale flowsheets.

Improving computational efficiency is important to analyze and optimize a complex system. The EO approach is preferred over the SM approach for handling large-scale complex flowsheets with nested recycle loops and implicit design specifications. In the latter, problems are solved iteratively by "tearing" the recycle streams in which an optimizer is coupled with a simulator.[13] In the former, all equations and variables that describe the unit operations are simultaneously solved.[14] The EO approach is superior to the SM approach if the Jacobian and Hessian matrices are directly available. In addition, EO modeling realizes powerful decomposition methods for large-scale problems.[15,16] The difficulty in applying the EO approach to air separation depends on the thermodynamics calculation because the equation-of-state (EOS) method mainly requires solving a cubic equation,[17,18] the roots of which are computed under logical if-else conditions, resulting in gradient discontinuity. Therefore, Kamath et al.[19] proposed a general EO approach to handle the cubic EOS by selecting the appropriate root in accordance with the desired phase. Recently, Dowling et al.[20] have discussed the presence of false equilibrium solutions in the supercritical region following the approach proposed by Kamath et al.[19] and then modified the cubic EOS model. Dowling et al.[21] optimized cryogenic systems for coal oxycombustion power generation. These studies also presented a framework[22] for efficient large-scale flowsheet optimization,

Received: July 27, 2015
Revised: November 6, 2015
Accepted: November 12, 2015
Published: November 12, 2015

DOI: 10.1021/acs.iecr.5b02768
Ind. Eng. Chem. Res. 2015, 54, 12096−12107

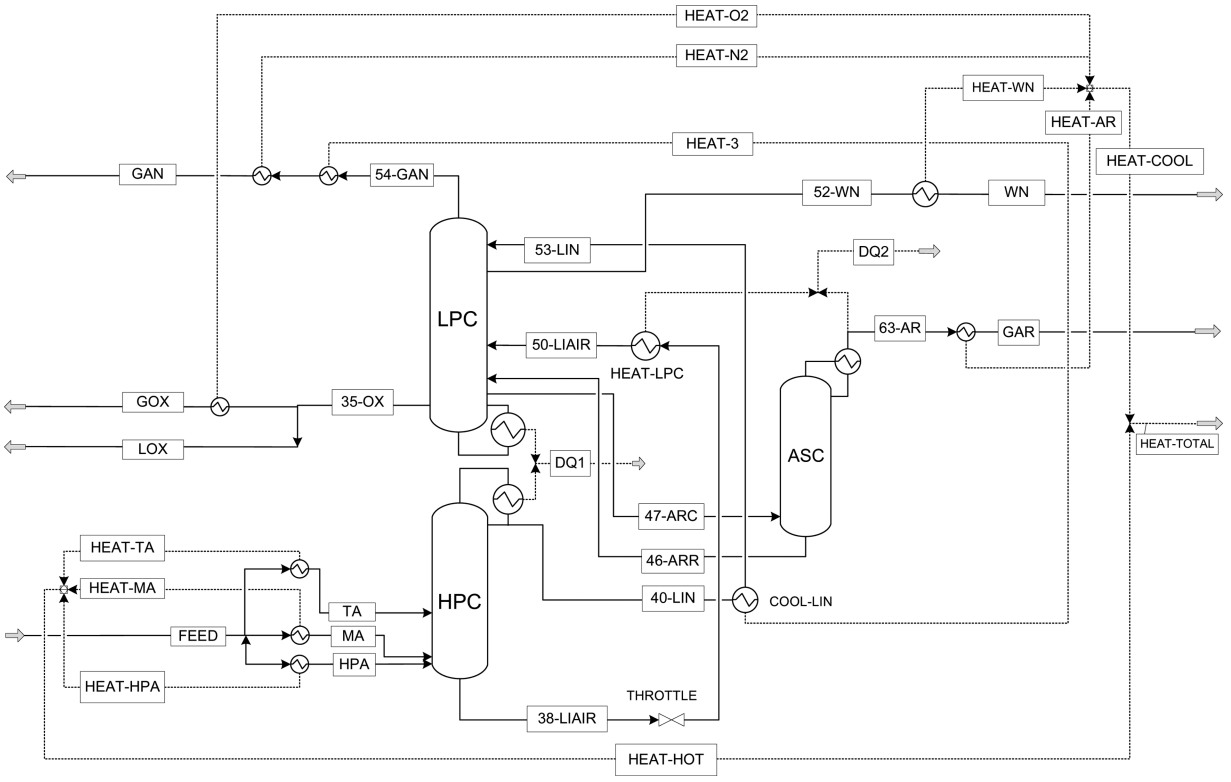

Figure 1. Flow diagram of the cryogenic air separation unit.

which combines advanced process optimization formulations with state-of-the-art algorithms.

In this study, a complete EO model is developed for cryogenic air separation. Compared with previous work, the present study addresses three issues of the ASU, namely, thermodynamic parameter estimation, process analysis with thermo-coupling design, and process optimization with varying load demands. An argon column is also introduced, which adds complexity to process analysis and optimization. The proposed EO method demonstrates a superior converging performance to the SM method.

2. EO FORMULATION FOR ASU FLOWSHEET

This study focuses on the process analysis and optimization of typical cryogenic air separation. The process flowsheet is shown in Figure 1. The process consists of three distillation columns, namely, a low-pressure column (LPC), a high-pressure column (HPC), and an argon side arm column (ASC). The following four products with impurities at the ppm level are generated: gaseous oxygen (GOX), liquid oxygen (LOX), gaseous nitrogen (GAN), and gaseous argon (GAR). Three fractions of clean air, that is, high-pressure air (HPA), main air (MA), and turbine air (TA), are sent into the HPC after being cooled and compressed to specific states. The air is separated into a high-purity liquid nitrogen and an oxygen-rich liquid stream in this column. These streams are then throttled and fed into the LPC for further distillation and production of high-purity GAN at the top and LOX at the bottom. The majority of the liquid oxygen is withdrawn as a liquid oxygen product, and the remainder is pumped and vaporized into GOX. The waste nitrogen (WN) is extracted as a reflux in the main heat exchanger to contribute to a cooling capacity. The third column ASC is designed to produce GAR at the top and return the oxygen-rich liquid to the LPC at the bottom.

As shown in Figure 1, two heat integration strategies are employed in the design to minimize energy consumption: (1) HPC and LPC are designed to share a common condenser/reboiler, that is, the condensing stream at the top of the HPC provides heat to the liquid at the bottom of the LPC; and (2) the bottom stream of the HPC, liquid air 38-LIAIR, is designed to provide a condensing duty for the ASC after throttling. Energy consumption is reduced through the heat coupling design at the cost of complications encountered during process analysis and optimization. To simplify the calculation, a coupled heat exchanger is usually simulated as two separate units, and the heat difference between the two units is minimized toward zero as much as possible. Therefore, two heat streams are used to denote the heat coupling relation for the coupled heat exchangers. These heat streams are denoted as DQ1 and DQ2 with dotted lines in Figure 1.

As with other chemical processes, the cryogenic ASU is characterized by its large scale, nonlinearity, and strong coupling. Simulating and optimizing ASU present challenges in terms of efficiency and convergence. In the current study, the EO approach is applied to formulate a rigorous ASU model. Several case studies are conducted to demonstrate the excellent convergence performance of the model. Each tray in a distillation column facilitates separation; the liquid stream from the upper tray and the vapor stream from the lower tray meet at the tray, exchange heat and mass, and then separate from each other with enhanced purity. The ASU is formulated with a rigorous tray-by-tray MESH model that consists of the component mass balance (eq 1), equilibrium equation (eq 2), summation equation (eq 3), and enthalpy balance (eq 4) of three components at the N stages.

$$L_{j-1}x_{j-1,i} + V_{j+1}y_{j+1,i} + F_jx_{Fi} = L_jx_{j,i} + V_jy_{j,i} \quad (1)$$

DOI: 10.1021/acs.iecr.5b02768
Ind. Eng. Chem. Res. 2015, 54, 12096−12107

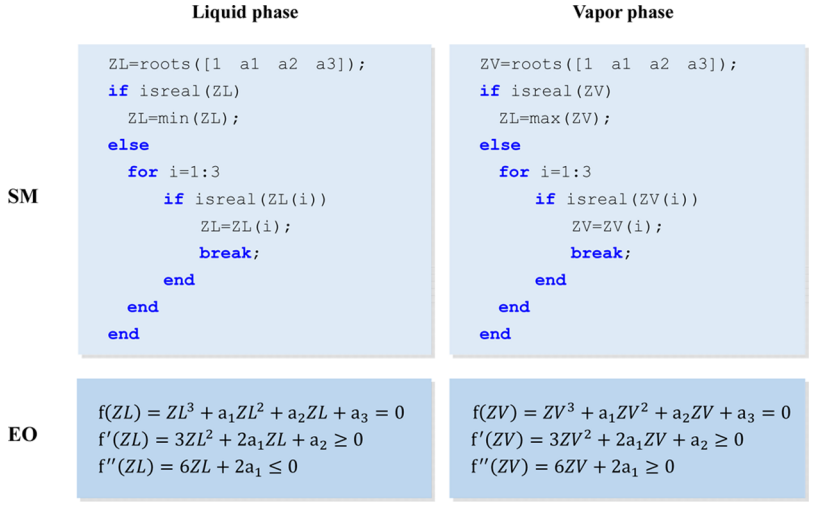

Figure 2. Comparison of liquid and vapor compression factor calculation using the SM and EO methods.

$$y_{j,i} = K_{j,i}x_{j,i} \tag{2}$$

$$\sum_{i=1}^{C} x_{j,i} = 1, \quad \sum_{i=1}^{C} y_{j,i} = 1 \tag{3}$$

$$L_{j-1}H_{L,j-1} + V_{j+1}H_{V,N+1} = L_jH_{L,j} + V_jH_{V,j} + Q_j \tag{4}$$

$$i \in \{N_2, Ar, O_2\}, \quad j \in \{1, ..., N\}$$

where i is the component index and j is the tray index. The equilibrium constants $K_{j,i}$ and the enthalpy of streams in the liquid and vapor phases ($H_{L,j}$ and $H_{V,j}$) are obtained using the thermodynamic property method.

In this study, the Peng−Robinson (PR)[17] cubic equations of state (CEOS) are integrated into the thermodynamic method for modeling. This method is founded in the EOS of van der Waals and can effectively predict thermodynamic properties through its reliable mixing rules and alpha functions. The thermodynamic method is widely used because of its advantages, including simple application, convenience, and low parameter requirements. Details of the PR model calculation are presented in Appendix A. As in the PR model, the following cubic equation holds for the compression factor:

$$z^3 + a_1z^2 + a_2z + a_3 = 0 \tag{5}$$

Obtaining the correct cubic equation roots is essential in the thermodynamic calculation. Eq 5 yields three roots, one of which is always real, whereas the other two roots could be real and distinct, real and nonunique, or imaginary. Depending on the number of real roots, each phase may either be in the one-root or three-root region. This phenomenon is discussed in a recent study by Dowling et al.[20] Eq 5 is formulated for both the liquid and vapor phases; thus, one phase may be in the three-root region, and the other may be in the one-root region for any given T, P, and x (y). If three real roots are involved, the largest root represents the compression factor of the vapor phase, whereas the smallest root represents the liquid phase. If only one real root exists then such is the desired root for the given phase. To this end, the most extensively used method is based on an analytic calculation that involves if-else loops, as shown in Figure 2. The upper two blocks illustrate the pseudocode for deriving the liquid and vapor compression factors by using the traditional SM method. Although a solution can easily be obtained, the presence of such loops results in discontinuous derivatives, which may generate problems for simulation and optimization in an EO framework.

Considering the difficulties that accompany procedure-based analytic calculations, Kamath et al.[19] and Dowling et al.[20] proposed a method of selecting the appropriate CEOS root based on the EO approach. The proposed method uses the mathematical properties of the cubic equation in combination with physical insights regarding the nature of vapor and liquid roots. The first- and second-derivative constraints of the cubic equation exhibit several regularities that can be applied to isolate and determine the desired roots. On the basis of the derivative properties of the vapor and liquid roots, a precise mathematical definition is developed; this definition can be adopted when solving thermodynamic models in accordance with the CEOS and is expressed as follows:

$$f(z_L) = 0, \quad f'(z_L) \geq 0, \quad f''(z_L) \leq 0 \tag{6}$$

$$f(z_V) = 0, \quad f'(z_V) \geq 0, \quad f''(z_V) \geq 0 \tag{7}$$

where z_L and z_V are the CEOS roots in the liquid and vapor phases, respectively. The effectiveness of the derivative-based constraints is verified by several numerical cases based on flash vessels and distillation columns.

In this study, air separation using the thermodynamic property method based on the PR CEOS is formulated by following the EO framework. The basic thermodynamic calculation model remains unchanged, as described in Appendix A; however, the if-else judgment is replaced with the derivative constraints expressed in eqs 6 and 7. The lower two blocks in Figure 2 illustrate the implementation of EO equations for the ASU process in comparison with the SM method. Thermodynamic calculation is performed on a ternary system composed of nitrogen, oxygen, and argon to validate the accuracy of the EO-based PR method. The calculation is based on a distillation column in air separation, and the results are compared with those of Aspen Plus, in which the equivalent thermodynamic model is embedded. The constants for physical and thermodynamic properties are retrieved from the physical database of Aspen Plus. Given the temperature, pressure, and mole flow rate of streams in the vapor and liquid phases throughout the column under specified conditions, the equilibrium constants and enthalpies can be obtained with

DOI: 10.1021/acs.iecr.5b02768
Ind. Eng. Chem. Res. 2015, 54, 12096−12107

EO formulations for PR functions, as introduced previously. The results are depicted in Figures 3 and 4. The distribution

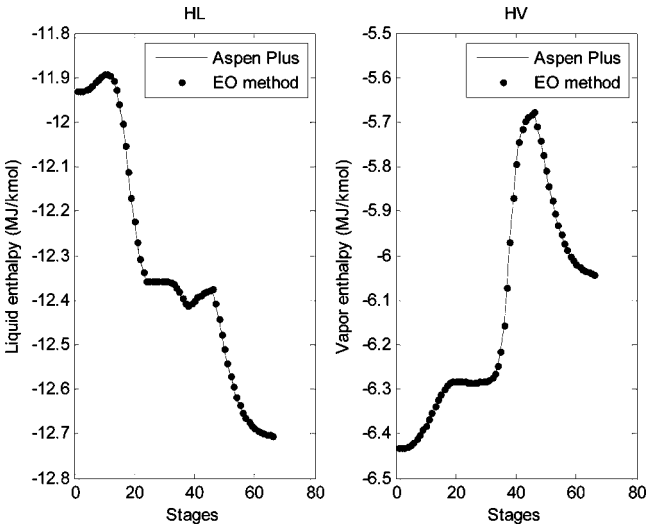

Figure 3. Comparison of the enthalpy calculation results.

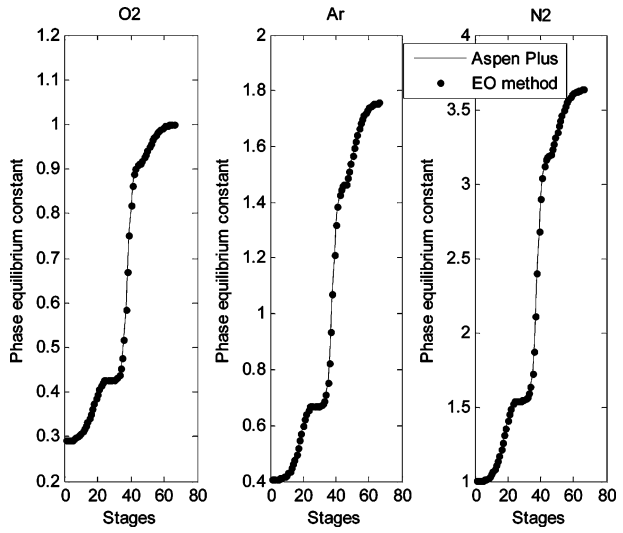

Figure 4. Comparison of the equilibrium constant calculation results.

results of the complete EO model overlap with the results obtained with Aspen Plus, thus validating the accuracy of the PR thermodynamic method in an EO framework.

On the basis of the EO formulations for the ASU model, the following three sections are presented to demonstrate the advantage of the EO method through different aspects of process analysis and optimization. The EO method is run with AMPL (32-bit version) and Interior Point OPTimizer version 3.8.1. The tolerance is set to 1×10^{-06}. The SM approach with Aspen Plus V7.2 is also used for the comparison study. The SQP algorithm is selected for the SM simulation in Aspen Plus, with the tolerance set to 1×10^{-05}. All computations are conducted on a PC with a 2.3 GHz Intel Core CPU, 6 GB memory, and Windows 7 system.

3. THERMODYNAMIC PARAMETER ESTIMATION

In the ASU process analysis, thermodynamic properties such as equilibrium constants and enthalpies must be determined. EO modeling facilitates the simultaneous calculation of the unit equations and the thermodynamic model. This study presents the advantage of EO modeling for thermodynamic parameter estimation. Binary interactive parameters (BIPs) describe the degree of interaction between two components in equilibrium. These parameters are highly significant for the accurate simulation of a chemical process. Three BIPs, k_{ij} ($i,j \in \{N_2, AR, O_2\}$, $i \neq j$), are included in this system. The original values retrieved from the Aspen Plus physical database fail to simulate the high purity requirement of the argon column. A new set of BIPs provided by the industry is adopted in this study. In this section, we demonstrate the advantages of the EO method over the traditional SM method in dealing with the parameter estimation using process data.

Aspen Plus with the new BIP setting is used to generate the process data. A parameter estimation task is then executed to evaluate whether or not the corresponding BIPs can be found with the generated data. This task can be converted to an optimization task. The objective is to minimize the concentration difference of the three components in n outlet streams between the generated distillation process data and the model-based prediction data. The three BIPs, k_{ij}, are the decision variables. The previous MESH equations and PR CEOS are used as constraints to represent the process model. The optimization problem is expressed as follows:

$$\min_{k_{ij}} \sum_{p=1}^{n} \sum_{q=1}^{3} \left(\frac{x_{p,q} - x^*_{p,q}}{x^*_{p,q}} \right)^2 \tag{8}$$

$$\text{s. t. : MESH equations for the flowsheet model} \tag{9}$$

$$\text{PR equations for the thermodynamic model} \tag{10}$$

where $x^*_{p,q}$ is the observed value of the mole fraction of component q in the outlet stream p from the distillation column and $x_{p,q}$ is the calculated value of the parameter estimation optimization problem.

The SM and EO methods are both tested for the parameter estimation. First, Aspen Plus is used for the SM test. The test involves two-nested loops, with the BIP search in the outer loop and the process simulation in the inner loop. The original BIPs from the Aspen Plus database are used as the initial guess for the optimization. The iterative results of the BIPs are shown in Figure 5 with a 3D plot. The curve with asterisks represents

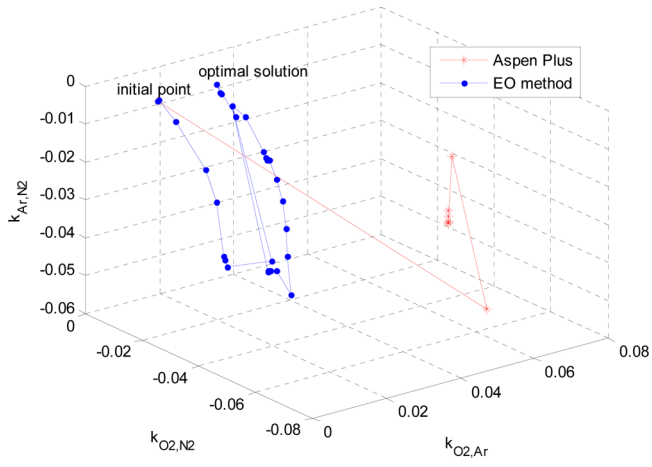

Figure 5. Comparison of BIP searching paths of the EO method and Aspen Plus.

DOI: 10.1021/acs.iecr.5b02768
Ind. Eng. Chem. Res. 2015, 54, 12096−12107

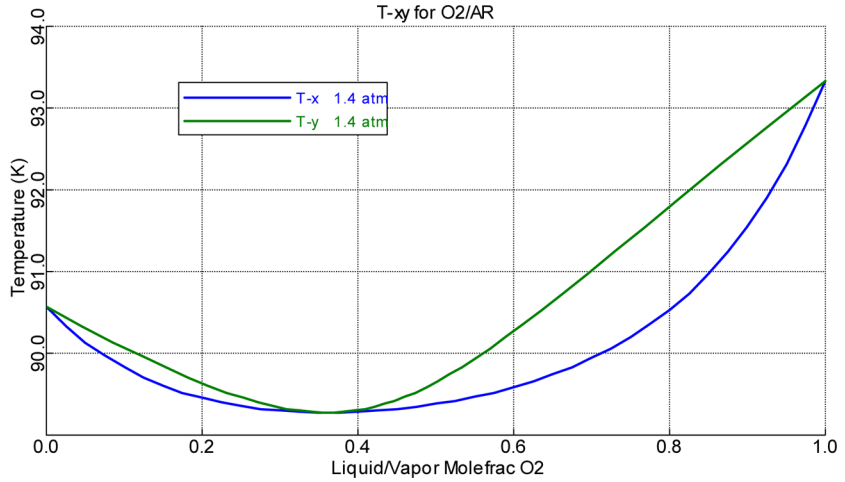

(a)

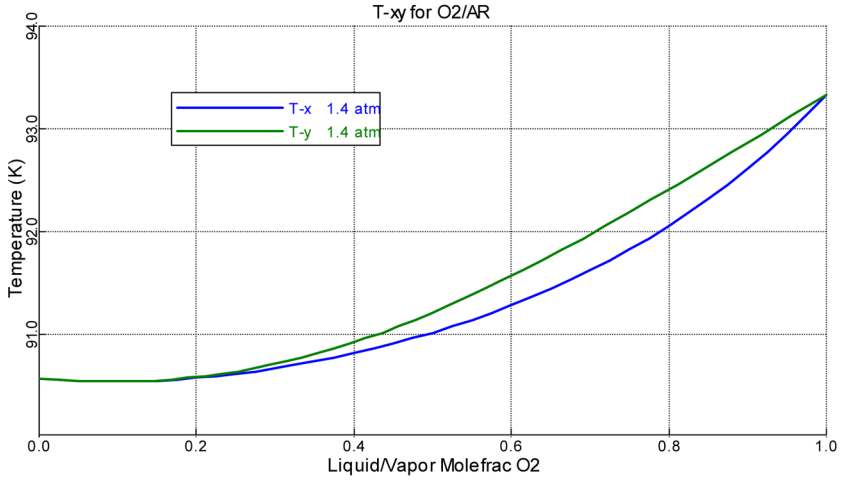

(b)

Figure 6. Comparison of the *T-x-y* vapor−liquid equilibrium diagrams of O_2−Ar. (a) BIPs set at the termination point of Aspen Plus. (b) BIPs set at the converged point obtained by the EO method.

the search path of BIPs calculated in Aspen Plus. The calculation fails after five iterations. The message shows that "the solver in this software can no longer handle the optimization problem." In addition, the test reveals that the failure does not depend on any algorithm settings such as the tolerance.

The EO method is subsequently tested. Aspen Plus also supports the EO mode, it cannot be applied to the BIP estimation because the thermodynamic model is not open in Aspen Plus. The complete EO method developed in this study is used. All EO variables are initialized with the Aspen SM results obtained at the BIPs provided by the Aspen Plus physical database. The results of the search path denoted by the curve with dots are also shown in Figure 5. After 40 iterations and a computational time of 2.167 s, the process successfully converged to the optimal solution, agreeing with the values used for the data generation.

To explain why Aspen Plus failed in this case, we further analyze the terminating point with the *T-x-y* Vapor−Liquid Equilibrium (VLE) diagram, as illustrated in Figure 6a. The dew point and bubble point curves meet at a point, indicating the existence of an azeotrope so that the mixture components can no longer be separated from one another at the current state. However, in reality, the azeotrope does not exist in air separation systems. This claim can be validated by observing the VLE diagram obtained by setting the BIPs at the converged point of the EO method, as shown in Figure 6b. The VLE diagram result reveals that the parameter estimation task executed in Aspen Plus traverses into an infeasible thermodynamic region wherein the desired separation is unachievable. Aspen Plus fails to continue the iteration under the nested iterative calculation wherein a thermodynamic model is embedded in the inner loop.

The previous results show that the SM method, unlike the EO method, is trapped into an infeasible thermodynamic region. The response of the EO method if it traverses into the infeasible thermodynamic region remains undetermined. To verify that the EO method is not dependent on luck, further testing is conducted using the EO method from the point where Aspen Plus failed. We set the BIPs of the EO model to the failed termination point and repeat the EO optimization. Figure 7 shows the BIP search path generated using the EO

DOI: 10.1021/acs.iecr.5b02768
Ind. Eng. Chem. Res. 2015, 54, 12096−12107

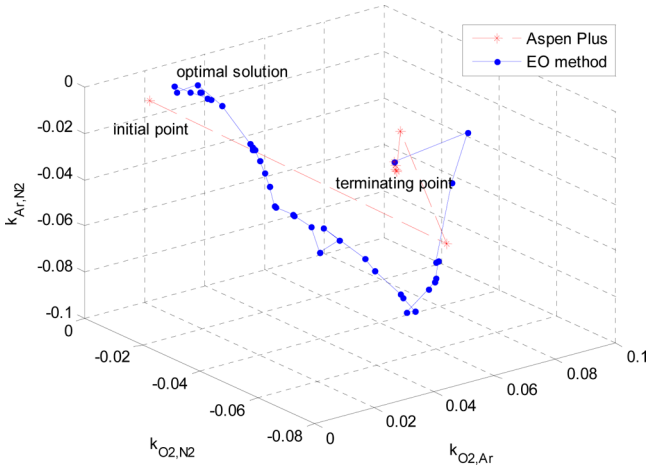

Figure 7. BIP searching path with a switch from Aspen Plus to the EO method.

method with the initials inherited from the terminating point of Aspen Plus. This time, the EO method performs 29 iterations and uses 1.442 s to successfully obtain the same optimal solution.

The different modeling methods of Aspen Plus and the complete EO approach, as presented in Figure 8, result in

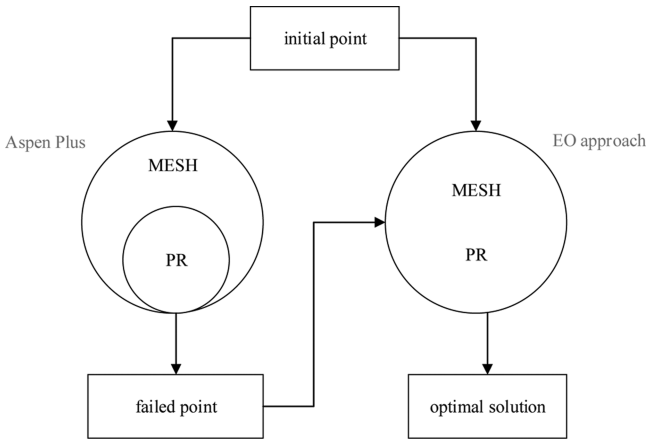

Figure 8. Illustration of the different modeling structures.

different calculation processes of the parameter estimation. The circle on the right represents the EO-based optimization model, in which the functions of the thermodynamic physical method are integrated with MESH functions. The AMPL platform allows the access to the first and second derivatives of all equations, including the CEOS, via automatic differentiation. Thus, an efficient large-scale nonlinear programming (NLP) algorithm that contributes to an excellent calculating performance can be applied in such an EO framework. On the contrary, the circle on the left represents the nested iterative calculation of Aspen Plus with its thermodynamic module embedded in the inner loop. The derivatives for the implicit models are not directly available and are typically determined based on a finite difference. Convergence is difficult to achieve using the Aspen Plus optimizer because of its round-off errors and the conventional procedure-based analytic calculation process applied in solving the CEOS.

We repeat the test with different initials to demonstrate that the trapping of Aspen Plus is not rare. As shown in Table 1, cases 1 to 4 compare the SM and EO methods. The EO method succeeds with the same optimal solution in each test. By contrast, Aspen Plus fails to solve the same problem, as described previously. The correct solution is obtained every time the search is switched to the EO method at the failed points. These results clearly demonstrate the advantage of the EO method over the traditional SM method in dealing with BIP parameter estimation.

Another test is also conducted to systematically explore the effect of different initial points on the BIP estimation with the EO method. The initial guesses of the three BIPs are extended to a wide range as $[-1, 1]$. The range of each BIP is evenly divided into 10 portions, and 11 equally spaced points are selected. Thus, a total of $11 \times 11 \times 11 = 1331$ BIP initials is obtained. Each time, we initialize the BIPs as one combination; the other variables are set to the initials of case 1. A total of 1331 estimations are finally tested with the EO method. The 3D plot in Figure 9 demonstrates the solving status of the 1331 estimations. The five-pointed star marks the optimal BIP point. The ● represents the successful initial points, and the ○ represents the ones that failed to converge. ○ are mainly located far from the optimal point, indicating that the EO method performs well when the initial point is not far.

In the previous test, all data are generated via simulation without any noise. Further testing is conducted by adding maximal 5% white noise to the measurement of case 1 to verify the robustness of the EO method. The results are presented as case 5 in Table 1. Comparison of cases 1 and 5 shows that the estimated parameters are slightly changed, proving the robustness of the EO method.

4. PROCESS ANALYSIS WITH THERMAL-COUPLING DESIGN

As shown in Figure 1, the complex flowsheet is designed for air separation. The process can be simulated given the total air feed information and the manipulated variables. The manipulated variables include the flow rate of the oxygen in LPC ($F_{35\text{-}OX}$), the flow rate of the liquid nitrogen reflux in HPC ($F_{40\text{-}LIN}$), the flow rate of the AR side draw in LPC ($F_{47\text{-}ARC}$), the flow rate of the WN side draw in LPC ($F_{52\text{-}WN}$), the flow rate fraction of the turbine air in the total air feed $[f_{TA} = F_{TA}/(F_{TA} + F_{HPA} + F_{MA})]$, the flow rate fraction of the high-pressure air $[f_{HPA} = F_{HPA}/(F_{TA} + F_{HPA} + F_{MA})]$ in the total air feed, the vaporization fraction of the heat exchanger HEAT−LPC ($\psi_{HEAT-LPC}$), the fraction of liquid oxygen in the total oxygen product $[f_{LOX} = F_{LOX}/(F_{LOX+GOX})]$, and the reflux ratio of ASC (R_{ASC}). All manipulated variables are listed in Table 2. Once the manipulated variables are fixed, all of the other process variables are theoretically determined through process simulation. The process analysis determines the suitable settings of the manipulated variables for the ASU process. The high-purity specifications of the products in this process are also listed in Table 2. The manipulated variables should be adjusted to meet the specifications. Meanwhile, the heat-coupling feature of this process should also be included in the simulation. This system includes two main heat integration designs: (1) HPC and LPC are designed to share a common condenser/reboiler, that is, the condensing stream at the top of the HPC provides heat to the liquid at the bottom of the LPC; and (2) the bottom stream of the HPC, liquid air 38-LIAIR, is designed to provide condensing duty for the ASC after the throttle. The coupled heat exchangers should ideally be simulated for the heat-integrated system. However, convergence is difficult to attain

DOI: 10.1021/acs.iecr.5b02768
Ind. Eng. Chem. Res. 2015, 54, 12096−12107

Table 1. BIP Estimation Results

			k_{O_2AR}	$k_{O_2N_2}$	k_{N_2AR}	status
case 1	initials		0.0104	−0.0119	−0.0026	
	results	EO model	0.0265	−0.01238	−0.004070967	converged
		AspenPlus	0.03389	−0.01142	−0.00264	calculations with errors
	EO from failed point		0.0265	−0.01238	−0.00407095	converged
case 2	initials		0.005	−0.025	−0.003	
	results	EO model	0.0265	−0.0123799	−0.00407092	converged
		AspenPlus	0.00400089	−0.0200044	−0.0125535	calculations with errors
	EO from failed point		0.0265	−0.01238	−0.00407095	converged
case 3	initials		0.097	−0.0012	−0.05	
	results	EO model	0.0264988	−0.0123792	−0.00406982	converged
		AspenPlus	0.04047486	−0.0553501	−0.0208633	calculations with errors
	EO from failed point		0.026499	−0.0123799	−0.00407088	converged
case 4	initials		0.0014	−0.02	−0.105	
	results	EO model	0.0264998	−0.0123799	−0.00407084	converged
		AspenPlus	0	−0.0873562	−0.074301	calculations with errors
	EO from failed point		0.0264998	−0.0123799	−0.00407084	converged
case 5	Initials		0.0104	−0.0119	−0.0026	
	EO results		0.0268	−0.01229	−0.00490983	converged

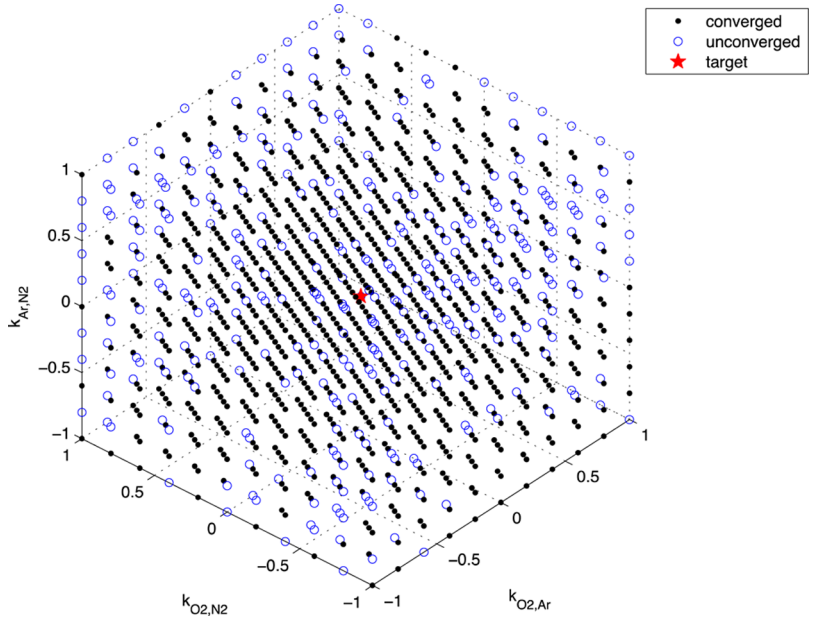

Figure 9. Solving status of BIP estimation problem with the EO method from different initial guesses.

with such a design in traditional commercial software. As dealt with in Aspen Plus, this process hardly converges with a complete thermal-coupling constraint while meeting high-purity product specifications. In practice, a coupled heat exchanger is replaced with two separate heat exchangers, and their heats are connected as two heat streams to observe the heat difference. As shown in Figure 1, the heat streams are denoted as dotted lines to distinguish them from the physical streams. The heat duties of the four units in the two pairs of thermally coupled design are also listed in Table 2: $Q_{condenserHPC}$ for the HPC condenser, $Q_{reboilerLPC}$ for the LPC reboiler, $Q_{condenserASC}$ for the ASC condenser, and $Q_{HEAT-LPC}$ for the preheater of the LPC, HEAT−LPC. DQ1 and DQ2 represent the heat residues between the two pairs of thermally coupled units, ideally with values equal to zero.

The thermal-coupling design of the heat-integrated distillation columns in cryogenic air separation can maximize heat/cooling integration and reduce overall energy consumption. However, the design also complicates the convergence of process simulation. The high purity specifications in this process narrow the feasible region and increase the difficulty of calculation. Establishing an operating condition that can meet all industrial specifications is challenging. If the heat-coupling specifications are enforced, Aspen Plus fails to find a feasible solution. The manipulated variables can be manually adjusted to reduce the heat difference while gradually meeting the high-purity product specifications; however, this manual approach depends on expert experience and is time-consuming. The best result obtained by the authors with Aspen Plus is listed in the third column of Table 2. The two pairs of thermally coupled units are not fully coupled in terms of heat residuals. In addition, the purities of some air products have not met the specifications under the operating conditions generated by

DOI: 10.1021/acs.iecr.5b02768
Ind. Eng. Chem. Res. 2015, 54, 12096−12107

Table 2. Comparison of the Simulation Results

		simulation in Aspen Plus	simulation with EO approach	Aspen Plus verification
manipulated variables	$F_{40\text{-}LIN}$ (kmol/h)	1665.251	1559.33	1559.33
	$F_{47\text{-}ARC}$ (kmol/h)	1058.343	1106.24	1106.24
	$F_{52\text{-}WN}$ (kmol/h)	1712.776	2130.97	2130.97
	$F_{35\text{-}OX}$ (kmol/h)	934.703	876.403	876.403
	f_{TA}	0.2771	0.3144	0.3144
	f_{HPA}	0.2772	0.2736	0.2736
	R_{ASC}	35	48.6982	48.6982
	$\psi_{Heat\text{-}LPC}$	0.53	0.594565	0.594565
purity specification	$y_{GOX,O2}$(≥0.999)	0.998[a]	0.9996	0.9996
	$y_{GOX,N2}$ (≤8 ppm)	4.21×10^{-10}	6.87×10^{-11}	6.78×10^{-11}
	$y_{GAN,O2}$ (≤8 ppm)	7.82×10^{-06}	7.88×10^{-06}	7.87×10^{-06}
	$y_{GAN,N2}$(≥0.9999)	0.9995[a]	0.9999	0.9999
	$y_{ARC,N2}$ (≤800 ppm)	3×10^{-03}	7.99×10^{-04}	7.87×10^{-04}
coupled heat (MJ/h)	$Q_{condenserHPC}$	−17134.13	−17139.63	−17151.20
	$Q_{reboilerLPC}$	17727.39	17139.63	17140.39
	$Q_{condenserASC}$	−6968.27	−7395.11	−7395.07
	$Q_{HEAT-LPC}$	6059.76	7395.11	7392.1
	DQ1	593.26[a]	0	−10.81
	DQ2	−908.51[a]	0	−2.97

[a]The purities of some air products.

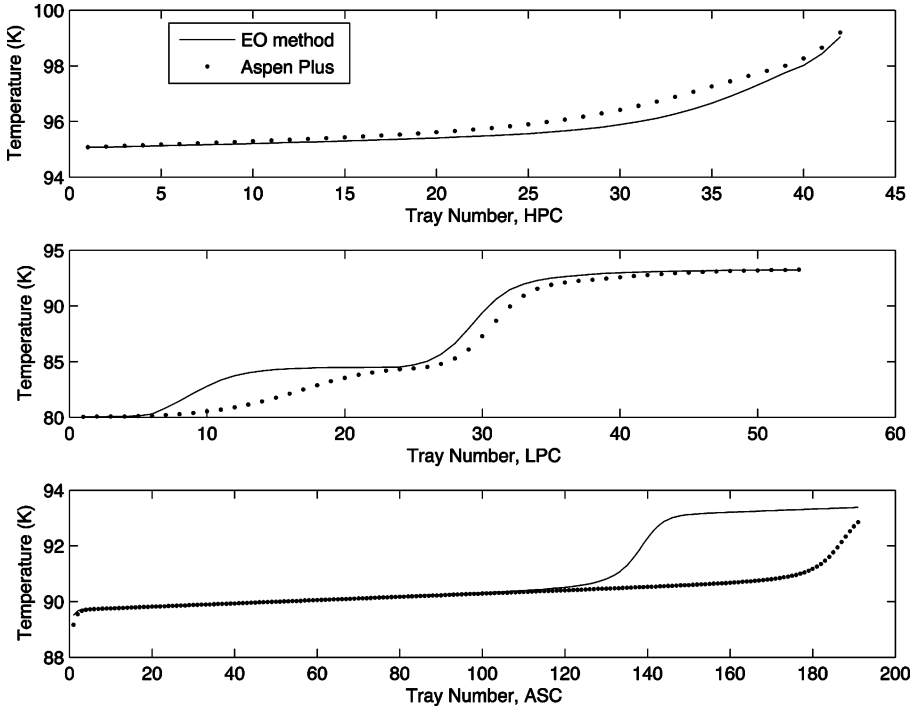

Figure 10. Comparison of the column temperature profiles of the EO method and Aspen Plus.

Aspen Plus. The violated constraints are marked with superscript *a* as shown in Table 2.

To avoid the tedious work of tuning the manipulated variables in the process analysis of the ASU, the following optimization problems can be formulated:

$$\min : eu + ep + du + dp \tag{11}$$

$$\text{s. t. } ep - eu = Q_{condenserHPC} + Q_{reboilerLPC} \tag{12}$$

$$dp - du = Q_{condenserASC} + Q_{HEAT-LPC} \tag{13}$$

$$\Delta T1 = T_{topHPC} - T_{bottomLPC} \geq 1.5\ \text{K} \tag{14}$$

$$\Delta T2 = T_{topASC} - T_{HEAT-LPC} \geq 3\ \text{K} \tag{15}$$

$$y_{GOX,O2} \geq 0.999 \tag{16}$$

$$y_{GOX,N2} \leq 8\ \text{ppm} \tag{17}$$

$$y_{GAN,O2} \leq 8\ \text{ppm} \tag{18}$$

$$y_{GAN,N2} \geq 0.9999 \tag{19}$$

$$y_{ARC,N2} \leq 800\ \text{ppm} \tag{20}$$

$$eu, ep, du, dp \geq 0 \tag{21}$$

DOI: 10.1021/acs.iecr.5b02768
Ind. Eng. Chem. Res. 2015, 54, 12096−12107

Flowsheet rigorous MESH models are provided (eqs 1−4). The equations of thermodynamics PR models are in Appendix A, where *eu*, *ep*, *du*, and *dp* are non-negative numbers that express the thermal-coupled unit design. The combination of the objective function (eq 11) and the first two constraints (eqs 12 and 13) is well-designed to generate the thermo-coupling feature of the process. The objective function can minimize the values of the four nonnegative variables to zero as much as possible; meanwhile, eqs 12 and 13 minimize the heat residues of the coupled heat pairs. Heat is fully coupled once the value of the objective function, which is expressed as $eu + ep + du + dp$, equals zero. At this point, the values of the heat residues, which are obtained using eqs 12 and 13, are also zero. Eqs 14 and 15 are attached as thermal-coupling constraints to ensure that heat is transferred from the hot stream to the cold stream. Eqs 16 to 20 are constraints that ensure high purity of the air products. The process models, including the flowsheet unit model based on the MESH equations and the thermodynamic model based on PR CEOS, are also included in the constraints.

With the above optimization formulation, the manipulated variables need not be adjusted manually. The optimal solution provides the best thermal-coupling design while meeting the high purity specifications. However, this formulation is difficult to implement without the EO modeling formulation. As in Aspen Plus, both SM and EO modes have difficulties in dealing with the constraints eqs 12−15. Meanwhile, the complete EO approach offers advantages in describing and solving this optimization problem. On the basis of the EO modeling idea, the built process model involves 10501 equations and 10509 variables. To simulate a process, the eight manipulated variables shown in Table 2 must be fixed. When the four auxiliary variables (*eu*, *ep*, *du*, and *dp*) and the two equalities (eqs 12 and 13) are introduced into the EO problem, the EO model considers 10503 equations and 10513 variables. Solver IPOPT 3.8.1 is used to calculate this large-scale optimization problem. With the Aspen Plus results in Table 2 as the initial guess, the optimal solution can be obtained after 149 iterations and a computational time of 30.18 s. The results are also presented in Table 2. The fourth column represents the process conditions generated by EO optimization. The two pairs of units are fully coupled, and the high purity requirements are met. The manipulated variables are altered to a certain extent in comparison with the previous condition. A comparison of the temperature profiles of each column between the two conditions is illustrated in Figure 10, which shows the deviations between the two conditions. To confirm the accuracy of the optimal results obtained using the proposed EO method, another process simulation is conducted in Aspen Plus by setting the manipulated variables at the optimal results and initializing the other variables with the EO solution. In this process, Aspen Plus converges successfully with the results, as listed in the last column of Table 2. The results in the last two columns are almost similar, indicating that the EO-based rigorous model describes the air separation process as precisely as Aspen Plus. In the current state, the purity and coupled heat are clearly improved compared with the previous Aspen results. The heat residues between the two pairs of thermally coupled units are very close to zero, indicating the extremely tight thermal coupling feature. In addition, all purity requirements are strictly satisfied.

The case study on determining the desired operating condition demonstrates the excellent convergence performance of the EO approach, particularly for such a large-scale NLP with strongly coupled variables and strict constraints. The EO-based model can precisely analyze the ASU process through CEOS-based thermodynamic calculation. In addition, the study highlights the convenience of switching from simulation to optimization with the EO model.

5. PROCESS OPTIMIZATION FOR VARYING LOAD DEMANDS

Operating condition fluctuation commonly occurs in industrial production. Load change is a frequently encountered scenario in which the industry aims to match changing customer demands by adjusting manipulated variables. This case is often observed in ASUs equipped to iron and steel plants because such processes are followed by batch operations. An ASU should change its operating point in line with varying loads to avoid oxygen release and thus save energy. The high-purity requirement should always be met during load change. Thus, the process should be optimized for varying load demands. Nonetheless, the operational optimization entails difficulty because of the large-scale, heat-coupling, and high-purity features of the process. This study addresses ASU optimization under oxygen load change by using the complete EO model. The results demonstrate the satisfactory convergence performance and fast computation capability of the EO approach.

Table 3. Computational Results of Optimization with Load Change

	gas oxygen load (Nm^3/h)					
	16000	17000	18000	19000	20,000	21000
time costs (s)	11.769	16.754	19.682	5.707	9.537	8.359
iterations	56	78	87	30	38	37

As oxygen load changes, the key variables of the process should be adjusted in a timely manner to ensure that the output of the process matches the demand. The same manipulated variables listed in Table 2 are chosen for optimization. Sales revenues and production cost are two main aspects considered in the industry. In this process, the energy consumption of three inlet streams is the main source of cost, and liquefied oxygen is the only product sold; the air products are for internal use in the steel plant in accordance with the load demand. Thus, the objective function of this optimization problem can be expressed as follows:

$$\text{objfun} = \sum_{i\in\{\text{OutStr}\}} F_i \times \text{price}_i - \sum_{j\in\{\text{FeedStr}\}} F_j \times \text{cost}_j \tag{22}$$

where {OutStr} represents liquefied oxygen; {FeedStr} represents a set of inlet streams, namely, TA, MA, and HPA; F_i or F_j denotes the flow rates of feed or product streams (kmol/h); price_i refers to the unit price of liquefied oxygen ($/kmol); and cost_j is the unit energy consumption of the three inlet streams ($/kmol).

The default oxygen load of the ASU is designed as 20000 N m^3/h. This load can vary from 16000 to 21000 N m^3/h as demanded. The other two gaseous products, nitrogen and argon, are constrained above a certain output level.

$$F_{\text{GOX}} = \text{oxygen load } (Nm^3/h) \tag{23}$$

$$F_{\text{GAN}} \geq 32000\ (Nm^3/h) \tag{24}$$

DOI: 10.1021/acs.iecr.5b02768
Ind. Eng. Chem. Res. 2015, 54, 12096−12107

Table 4. Key Variable Results of Optimization with Load Change

key variables		gas oxygen load (Nm^3/h)					
		16000	17000	18000	19000	20000	21000
purity specification	$y_{GOX,O2}$(≥0.999)	0.999	0.999	0.999	0.999	0.999	0.999
	$y_{GOX,N2}$(≤8 ppm)	$9.97e^{-11}$	$1e^{-10}$	$1.01e^{-10}$	$1.02e^{-10}$	$1.02e^{-10}$	$1.02e^{-10}$
	$y_{GAN,O2}$(≤8 ppm)	$7.99e^{-6}$	$5.62e^{-6}$	$3.78e^{-6}$	$2.76e^{-6}$	$2.13e^{-6}$	$1.73e^{-6}$
	$y_{GAN,N2}$(≥0.9999)	0.9999	0.9999	0.9999	0.9999	0.9999	0.9999
	$y_{ARC,N2}$(≤800 ppm)	$8e^{-4}$	$8e^{-4}$	$8e^{-4}$	$8e^{-4}$	$8e^{-4}$	$8e^{-4}$
coupled heat	DQ1	0	0	0	0	0	0
	DQ2	0	0	0	0	0	0
product flow rates (Nm^3/h)	F_{GOX}	16000	17000	18000	19000	20000	21000
	F_{LOX}	1817.06	1549.66	1602.34	1649.00	1692.61	1734.43
	F_{GAN}	32000	32000	32000	32000	32000	32000
	F_{GAR}	500.00	500.00	550.07	579.59	609.04	638.44
flow rates of key streams (kmol/h)	FEED	3880.63	4030.76	4252.07	4474.73	4698.06	4921.76
	$F_{40\text{-}LIN}$	1321.98	1381.05	1463.33	1543.89	1623.57	1702.71
	$F_{47\text{-}ARC}$	618.29	647.43	687.32	726.00	764.06	801.74
	$F_{52\text{-}WN}$	1634.33	1750.84	1923.84	2098.46	2273.88	2449.76
	$F_{35\text{-}OX}$	795.40	828.11	875.10	921.83	968.42	1014.93
	$F_{46\text{-}ARR}$	595.964	624.194	662.758	700.126	736.867	773.234
feed split ratios	f_{TA}	0.2557	0.1840	0.1745	0.1658	0.1579	0.1507
	f_{HPA}	0.2923	0.2990	0.3001	0.3010	0.3018	0.3024
reflux ratio vapor ratio	R_{ASC}	27.7932	27.9663	28.0966	28.1696	28.2145	28.2437
	$\psi_{Heat\text{-}LPC}$	0.4340	0.4369	0.4393	0.4407	0.4416	0.4422

$$F_{GAR} \geq 500\ (Nm^3/h) \tag{25}$$

The thermally coupled design is realized by minimizing the objective function expressed with auxiliary variables (eqs 12−13) in the process analysis section. However, these variables are restrained by equality constraints in this optimization problem as follows:

$$Q_{condenserHPC} + Q_{reboilerLPC} = 0 \tag{26}$$

$$Q_{condenserASC} + Q_{HEAT\text{-}LPC} = 0 \tag{27}$$

In addition to thermal-coupling and high purity constraints (eqs 14−21), other constraints of equipment and safe consideration on the flow rates of inlet streams are also included to ensure normal operation.

$$0.8\frac{F_{HPA}^*}{F_{GOX}^*} \leq \frac{F_{HPA}}{F_{GOX}} \leq 1.2\frac{F_{HPA}^*}{F_{GOX}^*} \tag{28}$$

$$0.6F_{FEED}^* \leq F_{FEED} \leq 1.5F_{FEED}^* \tag{29}$$

$$0.6(F_{HPA}^* + F_{TA}^*) \leq F_{HPA} + F_{TA} \leq 1.5(F_{HPA}^* + F_{TA}^*) \tag{30}$$

$$0.6F_{HPA}^* \leq F_{HPA} \leq 1.5F_{HPA}^* \tag{31}$$

$$0.6F_{TA}^* \leq F_{TA} \leq 1.5F_{TA}^* \tag{32}$$

Eq 28 is the safety consideration for the ratio between the HPA and GOX. Eqs 29−32 describe the upper and lower capacity limits of the each stage of the multistage compressor. The rigorous flowsheet model (eqs 1−4) and the thermodynamics model (Appendix A with eqs 6 and 7) are also included as constraints.

The optimization problem involves 10504 equations and 10511 variables. The difference between this model and the model in the previous section is that the flow rate of the gas oxygen is specified each time in accordance with the load change demand; the total air flow rate is also freed as a manipulated variable. In addition to the equations in the process model, eqs 26 and 27 are incorporated to define the heat-coupling specification. As indicated in Table 3, six cases with different GOX load demands are examined. Solver IPOPT 3.8.1 is applied to solve this large-scale NLP. The initials of this model are also from the Aspen Plus SM results, same as that used in the previous section on process analysis. The convergence results are listed in Table 3. The optimizations are successful in all cases. Moreover, the computational times and iterations of optimization differ under varied oxygen loads. Overall, the computational costs of handling such a large-scale, nonlinear, and strong-coupling optimization problem are less than 20 s, demonstrating the satisfactory convergence performance and high efficiency of the EO method.

As the oxygen load increases from 16000 to 21000 N m^3/h, the manipulated variables are adjusted in a specific range to meet the demand of output and operational specifications. The optimized results of the key variables for the six case studies are presented in Table 4. All cases converge to optimal solutions while satisfying the purity specifications and the heat-coupling design. On the basis of these key variables, several suggestions are prepared to guide operations: (1) ASC reflux ratio increases along with the vapor fraction of HEAT−LPC to compensate for the additional energy demand caused by the increase in feed air while maintaining the tight coupling of heat; (2) the ratio of liquid oxygen in the total oxygen outlets decreases as oxygen product load increases; and (3) the other flows of side-draw streams increase in correspondence with the rising feed air in the process.

6. CONCLUSIONS

In this study, ASU process analysis and optimization are conducted using the EO approach to achieve satisfactory convergence performance within an EO framework. The EO formulations, which include derivative-based constraints for PR CEOS thermodynamics, are implemented with several distillation columns. Parameters are then estimated to

DOI: 10.1021/acs.iecr.5b02768
Ind. Eng. Chem. Res. 2015, 54, 12096−12107

determine the accurate binary interaction factors that best fit this process. The essential difference in the convergences of EO and nested iterative calculation approaches is revealed with respect to handling complex chemical processes based on CEOS thermodynamics. Subsequently, air separation is analyzed on the basis of the thermal-coupling concept with an EO-based rigorous model. The effectiveness of this model is verified. The process with load change is optimized to confirm the excellent convergence performance and calculation speed of the EO approach. The study results demonstrate that the EO approach is advantageous in handling ASUs with large-scale, heat-coupling, and high-purity features.

APPENDIX A

Thermodynamic Model with PR Cubic Equation of States

Equation of state

$$P = \frac{RT}{v-b} - \frac{a}{v(v+b)+b(v-b)}$$

Mixing rules

$$b = \sum_i x_i b_i$$

$$a = \sum_i \sum_j x_i x_j (a_i a_j)^{0.5}(1-k_{ij})$$

$$b_i = 0.07789\frac{RT_{ci}}{P_{ci}}$$

$$a_i = 0.45724\alpha_i \frac{R^2 T_{ci}^2}{P_{ci}}$$

$$a_{ij} = (a_i a_j)^{0.5}(1-k_{ij})$$

$$a_L = \sum_i \sum_j x_i x_j a_{ij},\ a_V = \sum_i \sum_j y_i y_j a_{ij}$$

$$b_L = \sum_i x_i b_i, \quad b_V = \sum_i y_i b_i$$

Alpha functions

$$\alpha_i(T) = \sqrt{1 + m_i(1 - T_{Ri}^{0.5})}$$

$$m_i = 0.37464 + 1.54226\omega_i - 0.26992\omega_i^2$$

Cubic equations of state

$$Z_L^3 - (1-B_L)Z_L^2 + (A_L - 3B_L{}^2 - 2B_L)Z_L - (A_L B_L - B_L{}^2 - B_L{}^3) = 0$$

$$Z_V^3 - (1-B_V)Z_V^2 + (A_V - 3B_V{}^2 - 2B_V)Z_V - (A_V B_V - B_V{}^2 - B_V{}^3) = 0$$

$$A_L = \frac{a_L P}{R^2T^2}, \quad A_V = \frac{a_V P}{R^2T^2}, \quad B_L = \frac{b_L P}{RT}, \quad B_V = \frac{b_V P}{RT}$$

Fugacity constants functions

$$\ln(\phi_i^L) = \frac{b_i}{b_L}(Z_L - 1) - \ln(Z_L - B_L) - \frac{A_L}{2\sqrt{2}B_L} \times \left(2\frac{SL_i}{a_L} - \frac{b_i}{b_L}\right)\ln\left(\frac{Z_L + 2.414B_L}{Z_L - 0.414B_L}\right)$$

$$\ln(\phi_i^V) = \frac{b_i}{b_V}(Z_V - 1) - \ln(Z_V - B_V) - \frac{A_V}{2\sqrt{2}B_V} \times \left(2\frac{SV_i}{a_V} - \frac{b_i}{b_V}\right)\ln\left(\frac{Z_V + 2.414B_V}{Z_V - 0.414B_V}\right)$$

$$SL = a_{ij}^T x, \quad SV = a_{ij}^T y$$

Equilibrium constant

$$K_i = \frac{\phi_i^L}{\phi_i^V}$$

Enthalpy functions

$$\frac{(H_L - H_L^o)}{RT} = Z_L - 1 - \ln\left(\frac{Z_L + 2.414B_L}{Z_L - 0.414B_L}\right) \times \frac{\sum_i \sum_j x_i x_j A_L (1 + M_i + M_j)}{RT2\sqrt{2}B_L}$$

$$\frac{(H_V - H_V^o)}{RT} = Z_V - 1 - \ln\left(\frac{Z_V + 2.414B_V}{Z_V - 0.414B_V}\right) \times \frac{\sum_i \sum_j y_i y_j A_V (1 + M_i + M_j)}{RT2\sqrt{2}B_V}$$

$$H_L^o = \sum_{i=1}^N x_i H_i^o, \quad H_V^o = \sum_{i=1}^N y_i H_i^o, \quad M_i = \frac{m_i}{2}\sqrt{\frac{T_{Ri}}{\alpha_i}}$$

$$H_i^o = \Delta_f H_i^0 + \int_{T^{ref}}^T C_{Pi}\, dT$$

$$C_{Pi} = C_{i,1} + C_{i,2}\left(\frac{C_{i,3}/T}{\sinh(C_{i,3}/T)}\right) + C_{i,4}\left(\frac{C_{i,5}/T}{\cosh(C_{i,5}/T)}\right)$$

AUTHOR INFORMATION

Corresponding Authors

*E-mail: zhuly@zjut.edu.cn.

*E-mail: xichen@iipc.zju.edu.cn.

Notes

The authors declare no competing financial interest.

ACKNOWLEDGMENTS

We gratefully acknowledge the financial support from National Natural Science Foundation of China (Grant 21206149) and 973 Program of China (Grant 2012CB720503). We would also like to thank Professor L. T. Biegler at Carnegie Mellon University for the discussion and constructive suggestions on this work.

REFERENCES

(1) Agrawal, R. Production of ultrahigh-purity oxygen: A distillation method for the coproduction of the heavy key component stream free of heavier impurities. *Ind. Eng. Chem. Res.* **1995**, *34* (11), 3947.

DOI: 10.1021/acs.iecr.5b02768
Ind. Eng. Chem. Res. 2015, 54, 12096−12107

(2) Fu, C.; Gundersen, T. Using exergy analysis to reduce power consumption in air separation units for oxy-combustion processes. *Energy* **2012**, *44* (1), 60.
(3) Kansha, Y.; Kishimoto, A.; Nakagawa, T.; Tsutsumi, A. A novel cryogenic air separation process based on self-heat recuperation. *Sep. Purif. Technol.* **2011**, *77* (3), 389.
(4) Fu, Q.; Kansha, Y.; Liu, Y.; Song, C.; Ishizuka, M.; Tsutsumi, A. An advanced cryogenic air separation process for integrated gasification combined cycle (IGCC) systems. *Chem. Eng. Trans.* **2014**, *39*, 163−168.
(5) Rong, B. G.; Kraslawski, A.; Nyström, L. Design and synthesis of multicomponent thermally coupled distillation flowsheets. *Comput. Chem. Eng.* **2001**, *25* (4), 807.
(6) Rong, B. G.; Kraslawski, A.; Turunen, I. Synthesis of heat-integrated thermally coupled distillation systems for multicomponent separations. *Ind. Eng. Chem. Res.* **2003**, *42* (19), 4329.
(7) Huang, K.; Iwakabe, K.; Nakaiwa, M.; Tsutsumi, A. Towards further internal heat integration in design of reactive distillation columns—Part I: The design principle. *Chem. Eng. Sci.* **2005**, *60* (17), 4901.
(8) Huang, K.; Nakaiwa, M.; Tsutsumi, A. Towards further internal heat integration in design of reactive distillation columns—Part II. The process dynamics and operation. *Chem. Eng. Sci.* **2006**, *61* (16), 5377.
(9) Zhu, L.; Chen, Z.; Chen, X.; Shao, Z.; Qian, J. Simulation and optimization of cryogenic air separation units using a homotopy-based backtracking method. *Sep. Purif. Technol.* **2009**, *67* (3), 262.
(10) Sirdeshpande, A. R.; Ierapetritou, M. G.; Andrecovich, M. J.; Naumovitz, J. P. Process synthesis optimization and flexibility evaluation of air separation cycles. *AIChE J.* **2005**, *51* (4), 1190.
(11) Bian, S.; Khowinij, S.; Henson, M. A.; Belanger, P.; Megan, L. Compartmental modeling of high purity air separation columns. *Comput. Chem. Eng.* **2005**, *29* (10), 2096.
(12) Kamath, R. S.; Grossmann, I. E.; Biegler, L. T. Aggregate models based on improved group methods for simulation and optimization of distillation systems. *Comput. Chem. Eng.* **2010**, *34* (8), 1312.
(13) Biegler, L. T.; Grossmann, I. E.; Westerberg, A. W. *Systematic Methods of Chemical Process Design*; Prentice Hall: NJ, 1997.
(14) Westerberg, A. W.; Berna, T. J. Decomposition of very large-scale Newton-Raphson based flowsheeting problems. *Comput. Chem. Eng.* **1978**, *2* (1), 61.
(15) Zhu, Y.; Legg, S.; Laird, C. D. Optimal design of cryogenic air separation columns under uncertainty. *Comput. Chem. Eng.* **2010**, *34* (9), 1377.
(16) Zhu, Y.; Legg, S.; Laird, C. D. Optimal operation of cryogenic air separation systems with demand uncertainty and contractual obligations. *Chem. Eng. Sci.* **2011**, *66* (5), 953.
(17) Peng, D. Y.; Robinson, D. B. A new two-constant equation of state. *Ind. Eng. Chem. Fundam.* **1976**, *15* (1), 59.
(18) Soave, G. Equilibrium constants from a modified Redlich-Kwong equation of state. *Chem. Eng. Sci.* **1972**, *27* (6), 1197.
(19) Kamath, R. S.; Biegler, L. T.; Grossmann, I. E. An equation-oriented approach for handling thermodynamics based on cubic equation of state in process optimization. *Comput. Chem. Eng.* **2010**, *34* (12), 2085.
(20) Dowling, A. W.; Balwani, C.; Gao, Q.; Biegler, L. T. Optimization of sub-ambient separation Systems with Embedded Cubic Equation of State Thermodynamic Models and Complementarity Constraints. *Comput. Chem. Eng.* **2015**, *81*, 323.
(21) Dowling, A. W.; Balwani, C.; Gao, Q.; Biegler, L. T. Equation-oriented optimization of cryogenic systems for coal oxycombustion power generation. *Energy Procedia* **2014**, *63*, 421.
(22) Dowling, A. W.; Biegler, L. T. A framework for efficient large scale equation-oriented flowsheet optimization. *Comput. Chem. Eng.* **2015**, *72*, 3.

DOI: 10.1021/acs.iecr.5b02768
Ind. Eng. Chem. Res. 2015, 54, 12096−12107